

Synthesis and Properties of Biocompatible Water-Soluble Silica-Coated CdSe/ZnS Semiconductor Quantum Dots[†]

Daniele Gerion,^{*,‡,§} Fabien Pinaud,[§] Shara C. Williams,^{‡,§} Wolfgang J. Parak,^{‡,§}
Daniela Zanchet,[‡] Shimon Weiss,[§] and A. Paul Alivisatos^{‡,§,||}

Department of Chemistry, University of California, Berkeley, California 94720, and Materials Science Division, Lawrence Berkeley Laboratory, Berkeley, California 94720

Received: February 12, 2001; In Final Form: April 17, 2001

We describe the synthesis of water-soluble semiconductor nanoparticles and discuss and characterize their properties. Hydrophobic CdSe/ZnS core/shell nanocrystals with a core size between 2 and 5 nm are embedded in a siloxane shell and functionalized with thiol and/or amine groups. Structural characterization by AFM indicates that the siloxane shell is 1–5 nm thick, yielding final particle sizes of 6–17 nm, depending on the initial CdSe core size. The silica coating does not significantly modify the optical properties of the nanocrystals. Their fluorescence emission is about 32–35 nm fwhm and can be tuned from blue to red with quantum yields up to 18%, mainly determined by the quantum yield of the underlying CdSe/ZnS nanocrystals. Silanized nanocrystals exhibit enhanced photochemical stability over organic fluorophores. They also display high stability in buffers at physiological conditions (> 150 mM NaCl). The introduction of functionalized groups onto the siloxane surface would permit the conjugation of the nanocrystals to biological entities.

Introduction

Recent progress in wet chemistry has established a robust route toward the synthesis of highly luminescent semiconductor nanocrystals having sizes ranging from 1.5 to 8 nm.^{1,2} By judiciously controlling the growth conditions, the size, and even the shape of II–VI, nanocrystals can be accurately tailored.^{3,4} The ability to control these parameters has a profound impact in materials science since it can be harnessed for engineering assemblies of nanometer scale units with novel characteristics.^{5–8} At this point, the prominent focus has been the optical properties of these semiconductor nanocrystals. They are governed by strong quantum confinement effects and, therefore, are size dependent.^{2,9,10} The absorption onset and fluorescence emission shift to larger energy with decreasing size. Moreover, while the absorption spectrum is a continuum from the band gap into the UV, the emission pattern is narrow and symmetric and does not depend on the excitation frequency. Several different sizes of nanocrystals can thus be excited simultaneously with a single excitation source, resulting in well-resolved colors of emission. Further passivation of the nanocrystal surface by a thin shell of a higher band gap material does not significantly modify the absorption and emission features but increases the nanoparticle quantum yield up to 50–70%.^{11–13} The passivation shell also imparts an efficient photochemical stability, so that the photobleaching is reduced, and the number of photons a single nanocrystal can emit dramatically increases.

The ability to discriminate many different colors simultaneously under long-term excitation holds great promise for fluorescent labeling technologies, especially in biology.^{14,15} In this respect, organic dye molecules suffer from several limiting

factors. First, their narrow absorption bands make it difficult to excite several colors with a single excitation source. In addition, due to the large spectral overlaps between the emissions of dye fluorophores, multicolor imaging requires complex mathematical analysis of the data.¹⁶ Second, the emission intensity of organic dyes depends on their environment, and photobleaching imposes a stringent upper limit on the number of photons detectable per molecule. Third, the fast fluorescence emission of the dyes (<5 ns) coincides with a high degree to short-lived autofluorescence background from many naturally occurring species, reducing therefore the signal-to-noise ratio. In contrast, semiconductor nanocrystals emit light with a decay time on the order of a few tens of nanoseconds (~30–100 ns) at room temperature.¹⁷ The fluorescence decay is slower than the autofluorescence background decay, but fast enough to maintain a high photon turnover rate. Consequently, semiconductor nanocrystals might be ideal probes for spectrally multiplexed, time-gated cellular detection with enhanced selectivity and sensitivity.¹⁸

Highly luminescent nanocrystals with a narrow emission may be grown in hydrophobic inorganic surfactants. These high-quality monodispersed nanocrystals are insoluble in water and, therefore, are not compatible with biological systems. Alternative syntheses performed in aqueous solutions have been reported.^{19,20} They yield polydispersed nanocrystals that exhibit a broad trapped state emission that hides their advantage of well-resolved colors of emission. Several strategies have been pursued to solubilize high-quality hydrophobic nanocrystals in aqueous solvents.^{15,21,22} They rely on priming the nanocrystal surface with a thiolated molecule having a free carboxyl group facing the solution that warrants water solubility. In this case, the bond holding the primer to the nanocrystal is dynamic, leading to a low stability of the nanocrystals in water. Moreover, the chemical reactions may lead to slow dissolution of the CdSe/ZnS particles and to the diffusion of heavy atoms into the solution. To slow such a process, and to mask the toxicity of

[†] Part of the special issue "Royce W. Murray Festschrift".

* Corresponding author. E-mail: gerion@uclink4.berkeley.edu. Fax number: (510) 642 6911.

[‡] University of California.

[§] Lawrence Berkeley Laboratory.

^{||} E-mail: alivis@uclink4.berkeley.edu.

the nanocrystals for bioorganisms, a complete and robust encapsulation of the inorganic fluorophores is mandatory.^{14,19,20}

Guided by these considerations, we reported an alternative approach in which the core/shell nanoparticles are embedded in a polymerized silica shell.¹⁴ In this article we describe this synthesis in more detail. The procedure yields nanocrystals encapsulated in a silica shell of about 2–5 nm, functionalized with thiols and/or amines on the surface. The silanized (or silica-coated) nanocrystals are soluble in buffer solutions over a wide range of pH even at high salt concentrations (up to 200 mM), and they retain the optical properties of the original core/shell particles. We emphasize that silica-coated nanocrystals have a greater stability in biological buffers compared to nanoparticles primed with thiolated molecules such as mercaptopropionic acid, and this stability can justify the amount of effort spent producing them.

This article is organized as follows: in the first part, we describe the synthesis of silica-coated and mercaptopropionic acid-coated nanocrystals in detail. Next, we focus on the influence of the silica shell on the optical properties of the nanocrystals. Finally, we compare the size distribution and the chemical surface properties of both silica-coated and mercaptopropionic acid-coated CdSe/ZnS nanocrystals.

Experimental Section

A. Chemicals and Materials. Trioctylphosphine oxide (TOPO, #346187), mercaptopropyltris(methyloxy)silane (MPS, #175617), aminopropyltris(methyloxy)silane (APS, #281778), tetramethylammonium hydroxide in methanol (TMAH, #334901), and tetramethylammonium hydroxide pentahydrate (#223212), (trihydroxysilyl)propyl methylphosphonate in water (42% wt/wt, #435716), chlorotrimethylsilane (#386529), mercaptopropionic acid (MPA, #M5801), 4-(dimethylamino)pyridine (DMAP, #D5640), 5,5'-dithiobis(2-nitrobenzoic acid) (DTNB) were purchased from Sigma-Aldrich (Milwaukee, WI).

Dialysis tubing (MWCO = 10 000, #D9652) and Sephadex G25 medium (#G2580) were purchased from Sigma-Aldrich. Acrodisc syringe filters with 0.45 mm pore size nylon membrane (#PN4428T) were purchased from Pall Gelman Laboratory (Ann Arbor, MI). Centricon devices (YM-100 Centriplus, Millipore, San Jose, CA), NAP columns (#17-0852-01, Amersham Pharmacia, Piscataway, NJ), and dialysis cassettes (#66810, Slide-A-Lyzer, Pierce, Rockford, IL) were used as specified.

Buffers used in this study included phosphate buffer (PB, a mixture of K_2HPO_4 and KH_2PO_4 , #P8709 and #P8584, Sigma-Aldrich), 2-(*N*-morpholino)ethanesulfonic acid buffer (MES, #M5287, Sigma-Aldrich), and Tris–Borate–EDTA buffer (0.5 × TBE, #T3913, Sigma-Aldrich). The ionic strength was adjusted by adding a calibrated amount of NaCl.

B. Synthesis of Water-Soluble Semiconductor Nanocrystals. CdSe/ZnS core/shell nanocrystals were synthesized in TOPO following standard procedures described in the literature.^{1,11–13} The nanocrystals were stored at room temperature in a mixture of butanol/TOPO (ratio by volume ~1/2) with typical concentrations of 5–10 mg of CdSe cores per milliliter of solution and were stable for months. No special precautions were taken to prevent oxidation.

Silica-Coated Nanocrystals. A typical synthesis of silica-coated nanoparticles is described hereafter and schematically illustrated in Figure 1. The quantities can be easily scaled and apply for making CdSe/ZnS nanocrystals with any size between ~2 and 8 nm. One milliliter of nanocrystals in butanol/TOPO (optical density (OD) of nanocrystals ~ 2) was precipitated using anhydrous methanol. The wet precipitate was dissolved in 50

μ L of MPS. After vortexing, 5 μ L of TMAH in methanol was added, and the solution became optically clear. This mixture was diluted with 120 mL of anhydrous methanol basified to pH ~ 10 with 750 μ L of TMAH and put under N_2 in a 500 mL three-neck-flask. After 1 h of mild stirring, the solution was gently heated to ~60 °C for 30 min. After cooling to room temperature, 90 mL of methanol, 10 mL of 18 M Ω Millipore water, 600 μ L of (trihydroxysilyl)propyl methylphosphonate and 20 μ L of MPS were added, stirred for ~2 h, heated to ~60 °C for less than 5 min, and cooled to ~30 °C. The remaining silanol groups were quenched with a mixture of 20 mL of methanol and 2 mL of chlorotrimethylsilane basified with ~3 g of solid TMAH pentahydrate, and then stirred again for ~2 h. The solution was heated to ~60 °C for ~30 min, and then left at room temperature for 2–4 days while stirring in a N_2 atmosphere. In the next step, the solution was condensed by a factor of 2–5 in a rotary evaporator (Re111, Buchi, Flawil, Switzerland) and left again for 24 h. At this point, the solution was dialyzed in a 10 000 MWCO dialysis tubing against methanol for 1 day, and subsequently filtered through a 0.45 μ m pore size nylon syringe filter. The excess of free silane was removed by condensing the solution using centrifugal filter devices (YM-100 centriplus/centricon 100, MWCO 100 000). The volume of the solution was reduced to about 2 mL. The solution of silanized nanocrystals in methanol was left for at least 12 h before being passed through a solvent exchange column. We used either NAP columns or a homemade 20 cm long column with a 0.7 cm diameter filled with ~5 g of Sephadex G25 medium and equilibrated with 10 mM PB buffer, pH ~ 7. The eluted solution (~3 mL) was monitored by fluorescence and only the fluorescent fraction was collected. It was left a few hours and then was filtered through a 0.22 μ m pore size acetate filter. As an optional step, this solution was further dialyzed against 18 M Ω Millipore water (Millipore, San Jose, CA) for 1–4 days in a 10 000 MWCO membrane, run through a 0.22 mm pore size filter, and concentrated to a desired concentration in a vacufuge concentrator at 60 °C (#5301, Eppendorf, Westbury, NY). As a last step, the solution was centrifuged at 20000×*g* for 30 min and the precipitated was discarded. The supernatant was stored in air with typical optical densities at the absorption feature of ~0.3–1, corresponding to a concentration of 3–10 μ M (the extinction coefficient was taken as 10⁵ M⁻¹ cm⁻¹).

Mercaptopropionic Acid-Coated Nanocrystals (MPA-CdSe/ZnS). The MPA-coated nanocrystals were synthesized following the literature protocols.^{21,22} One milliliter of CdSe/ZnS in butanol/TOPO (OD of nanocrystals ~2) was precipitated with anhydrous methanol. The wet precipitate was then resuspended in a mixture of 1 mL of *N,N*-dimethylformamide (DMF) and 0.1 mL of 3-mercaptopropionic acid. This solution was vortexed and sonicated for ~10–30 min until it became transparent and then stored for 1–4 days at room temperature. In a next step, ~3–7 mL of 4-(dimethylamino)pyridine (DMAP) dissolved in DMF was added (~20 mg of DMAP in 1 mL of DMF). The solution turned cloudy and was centrifuged for 1 h at 3000×*g*. The supernatant was discarded while the precipitate was dried under nitrogen and then dissolved in 0.1–1 mL of 18 M Ω water. As a last step, the solution was centrifuged 30 min at 20000×*g*, and only the supernatant was used for experiments. To remove the excess of MPA, when necessary, the solution could be run through a NAP column that had been equilibrated with 18 M Ω Millipore H₂O.

For experiments performed in buffer solutions, the solvent of the nanocrystals was changed from water to the desired buffer

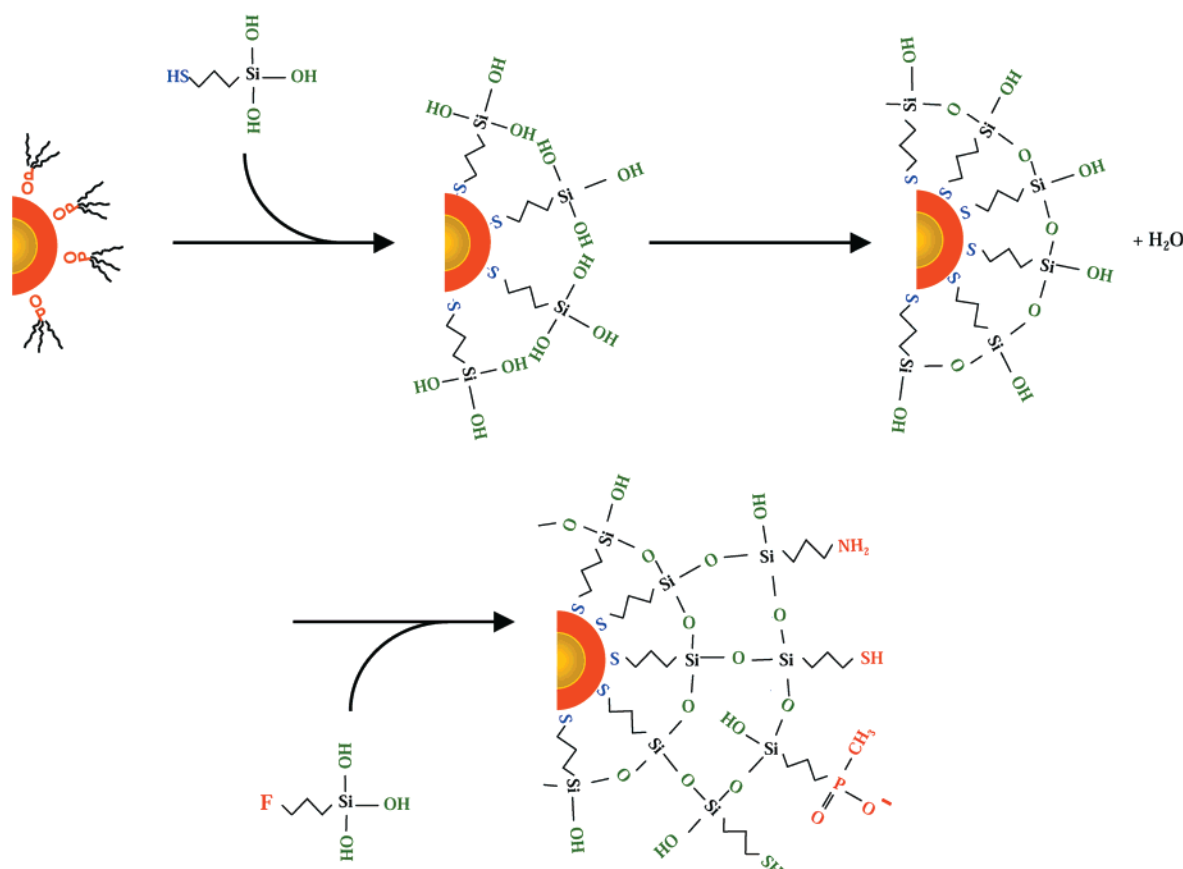


Figure 1. Sketch of the silanization method. The TOPO-capped CdSe/ZnS core/shell particles are dissolved in pure MPS, drawn in its hydrolyzed form for convenience in the figure. After basification, the MPS replaces the TOPO molecules on the surface. The methoxysilane groups ($\text{Si}-\text{OCH}_3$) hydrolyze into silanol groups ($\text{Si}-\text{OH}$), and form a primary polymerization layer. Heat strengthens the silanol-silanol bridges by converting them into siloxane bonds and releasing water molecules. Then, fresh silane precursors containing a functional group ($\text{F} = -\text{SH}$, $-\text{NH}_2$; $-\text{PO}(\text{O}^-)\text{CH}_3$) are incorporated into the shell and may tailor the nanocrystal surface functionality. In a last step (not shown) the remaining hydroxyl groups are converted in methyl groups; this last step blocks further silica growth.

solution using a NAP column, or by dialysis with a 10000 MWCO membrane, or simply by adding the concentrated buffer.

C. Photophysical Characterization. UV-vis absorption spectra were carried out using a HP8453 diode array spectrometer (Hewlett-Packard, Palo Alto, CA). Core/shell, silanized, and MPA-coated nanocrystal solutions were placed in a 2 mm path length quartz cuvette. The fluorescence emission was measured with a Spex 1681 0.22 m/0.34 m spectrometer (Spex, Edison, NJ). For the room-temperature quantum yield determination, we compared the integrated peak emission intensity of the silanized nanocrystals in 10 mM PB to the emission of rhodamine 6G in water (quantum yield, $\text{QY} = 95\%^{24}$) of an identical OD of 0.15 at 480 nm, the excitation wavelength.

The photostability of silanized nanocrystals has been investigated in two sets of experiments. To probe the stability of the fluorescence over time, 1 mL of diluted silanized nanocrystals in 10 mM PB buffer ($\text{OD} = 0.01$ at the exciton peak) was excited at 340 nm and the integrated fluorescence intensity was recorded in four subsequent measurements. The mean area of the emission peak was computed and normalized to the value of day 1. To probe the photostability under continuous Ar^+ laser excitation, a thin quartz cuvette was filled with 1 μL of silanized nanoparticles or dye molecules with an identical OD of 0.065 at 488 nm. The cuvette was mounted on a epifluorescence microscope (Axiovert S100TV, Zeiss, Oberkochen, Germany) and excited at 488 nm with a 0.5 mW cw Ar^+ laser focused on a spot of 700 μm . The integrated fluorescence intensity of a region of interest of $\sim 10 \mu\text{m} \times 10 \mu\text{m}$ was recorded for 4 h at intervals of 5 s and normalized to its initial value.

D. Size Characterization. The size of core/shell CdSe/ZnS particles was investigated using a high-resolution transmission electron microscope (either Topcon EM002B at 200 keV or JEM-3010 ARP at 300 keV). Approximately 5–10 μL of nanocrystals in toluene, chloroform, or water ($\text{OD} \sim 0.3$) was spread on an ultrathin carbon-coated grid and dried in air. Images were either obtained with a CCD camera (Gatan, MSC 794) or digitized afterward, and the diameter of the particles was determined by using standard image processing softwares.

As an additional technique for the determination of the silica shell size, we used electron energy loss spectroscopy (EELS, TEM-CM200FEG microscope). Samples of silanized nanoparticles ($\sim 10 \mu\text{L}$) were deposited on a 400 mesh carbon-coated grid and allowed to dry overnight. EELS spectra were recorded at the absorption band edge of Si (110 eV) and at the absorption band edge of the Se atoms (67 eV).

Visualization of the silica shell by HRTEM was difficult (see Results). The sizes of silanized and MPA-coated nanocrystals were therefore measured using atomic force microscopy (AFM). About 10 μL of water-soluble nanocrystals was spread on a freshly cleaved mica surface, incubated 10 min, gently rinsed with 3 drops of water, and dried under a flow of nitrogen. Images were recorded in “tapping mode” in air, using a MultiMode AFM and TESP cantilevers (Digital Instrument, Santa Barbara, CA). The height of the particles was obtained from the recorded images; all features were counted in the histograms. For each sample, more than 500 dots were considered in the statistics.

To obtain more information about the size distribution of the

silanized nanocrystal solutions, high-performance liquid chromatography (HPLC) was performed on a 30 cm long size exclusion column (G4000-SWx1, TSK-gel, Supelco, Bellefonte, PA). The column was packed with a silica-based phase composed of 7 μm beads of pore size of 45 nm. We loaded an aliquot of 20 μL of silanized nanocrystals in 10 mM PB (OD ~ 0.1) that eluted through the column at a flow rate of 0.5 mL/min in 10 mM PB, 50 mM NaCl, pH ~ 7 . The eluting solution was monitored in time by its absorption at 210 nm.

E. Surface Characterization and Solubility. The number of reactive thiols on the silanized nanocrystal surface was determined by the Ellman's reagent method.²⁵ 5,5'-dithiobis-(2-nitrobenzoic acid) (DTNB) was added to nanocrystals dissolved in 50 mM PB, pH = 7.3, to a final concentration of 1–10 mM. This solution was incubated for 2 h at room temperature. The absorption spectra of this solution and a similar nanocrystal solution without DTNB were measured and compared. The concentration of nanocrystals was determined from absorbance, assuming a nanocrystal extinction coefficient of 100 000 $\text{M}^{-1} \text{cm}^{-1}$ at the first exciton peak. The concentration of free thiols was derived from the difference in the absorbances at 412 nm of the solutions with and without DTNB, using an DTNB extinction coefficient of 13 600 $\text{M}^{-1} \text{cm}^{-1}$.

Gel electrophoresis was employed to investigate the surface charge properties and the stability of water-soluble nanocrystals in various salt concentrations (Sub-Cell GT agarose gel electrophoresis system, BioRad, Hercules, CA). Agarose gels (1 to 3%) were cast in different buffers (PB pH ~ 7 , MES pH ~ 5.5 , 0.5 \times TBE pH ~ 8.6). A 20 μL aliquot of the nanocrystal solution was mixed with 4 μL of 30% (wt/wt) glycerin in buffer, and the mixture was briefly vortexed and loaded in the wells. Typical voltages of 50–100 V (3.3–6.7 V/cm) were applied over 30–120 min. The detection of the nanocrystals in the gel was performed by illuminating the gels with a UV table (2020E UV/White transilluminator, Stratagene, LaJolla, CA) and recording the fluorescence images with a CCD camera (EagleEye-II software, Stratagene). To compare the salt stability of silica and MPA-coated nanocrystals, different amounts of NaCl were added to nanocrystal samples dissolved in 30 mM PB, resulting in final NaCl concentrations of 1000, 500, 200, 100, 50, 20, 10, 5, 1, and 0 mM NaCl. After 5 h of incubation, the nanocrystals were run in a 1% agarose gel (30 mM PB, no NaCl) and detected as described above.

Electrophoresis was also used to select narrow bands corresponding to nanocrystals with a narrow distribution in their size-to-charge ratios. We followed the step by step procedure detailed in ref 26. The "band narrowing" was performed in TBE buffer.

Results

A. Photophysical Characterization. The absorption and emission spectra of the silanized nanoparticles in 10 mM PB buffer are shown in Figure 2 and can be compared to the spectra of CdSe/ZnS dots in toluene (inset). The data are summarized in Table 1. The silica shell does not significantly change the absorption spectrum of the core/shell CdSe/ZnS particles inbetween 450 and 720 nm. The emission pattern of silanized nanocrystals is close to that of core/shell particles in toluene. The peak is symmetric and, unlike dye fluorophores, does not exhibit a red tail. Full width at half-maximum (fwhm) values of ~ 32 nm are obtained, enabling effective distinction between the different colors of emission. We observe a 1–2 nm red shift of the fluorescence emission peak of the silanized particles in water compared to the same samples in toluene. The global Stokes shifts are about 20 nm for all sizes. Absolute quantum

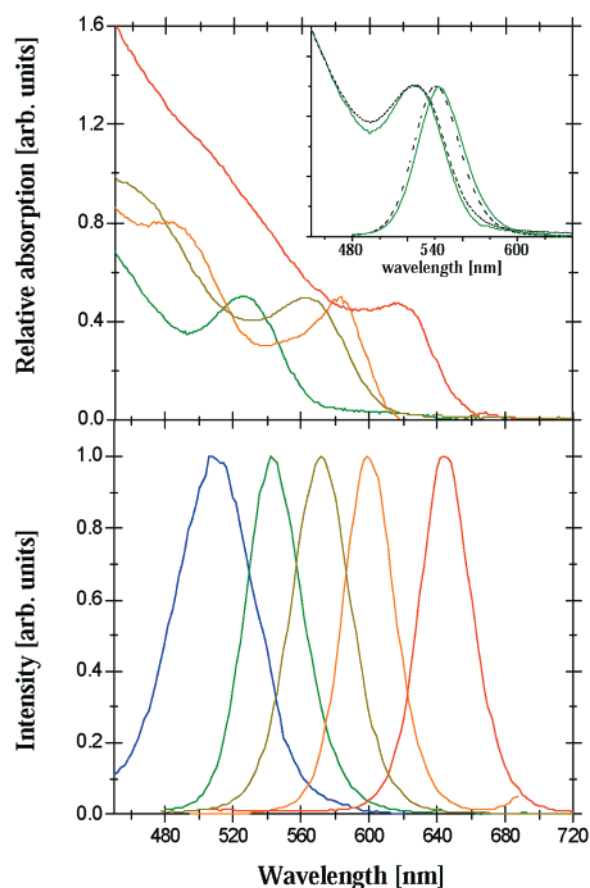


Figure 2. Absorption (upper panel) and emission (lower panel) spectra of a series of silanized CdSe/ZnS in 10 mM PBS buffer, pH ~ 7 . The data are normalized for the convenience of the display. From right to left, red, orange, yellow, green, and blue emitting nanocrystals are shown. For blue emitting particles, the absorption spectrum does not show features above 450 nm and is therefore omitted. Inset: Absorption and emission of silanized green nanocrystals in 10 mM PB (solid lines), and of the same green CdSe/ZnS particles in toluene (dashed lines).

TABLE 1: Summary of the Optical Properties of the Silica-Coated CdSe/ZnS Nanocrystals^a

color of fluorescence of the silanized nanocrystals	absorption peak (nm)	emission peak (nm)	quantum yield (QY)	QY relative to CdSe/ZnS nanocrystals
blue		504		
green	522	544	18%	81%
yellow	560	576	12%	66%
orange	576	595	9%	60%
red	620	644	5%	71%

^a The absorption of blue nanocrystals does not show a distinct peak, and it is therefore not determined. Accordingly, the quantum yield could not be measured.

yields (QY) of 18%, 12%, 9%, and 5% are obtained for nanocrystals with green (542 nm), yellow (572 nm), orange (595 nm), and red (644 nm) emission respectively, although the exact QY varies slightly for different silanization synthesis of the same CdSe/ZnS nanocrystals. Importantly, the QY remains about ~ 60 –80% of the initial QY of the CdSe/ZnS nanoparticles in toluene.

As shown in Figure 3, the QY of the silanized nanoparticles in 10 mM PB buffer is remarkably constant over time, showing only a slight decrease of approximately 1–5% over a period of 1 month. Similar behavior has been observed for three different colors of nanocrystals in a buffer solution. No noticeable variations of the QY with pH ($6 < \text{pH} < 8$) are observed over

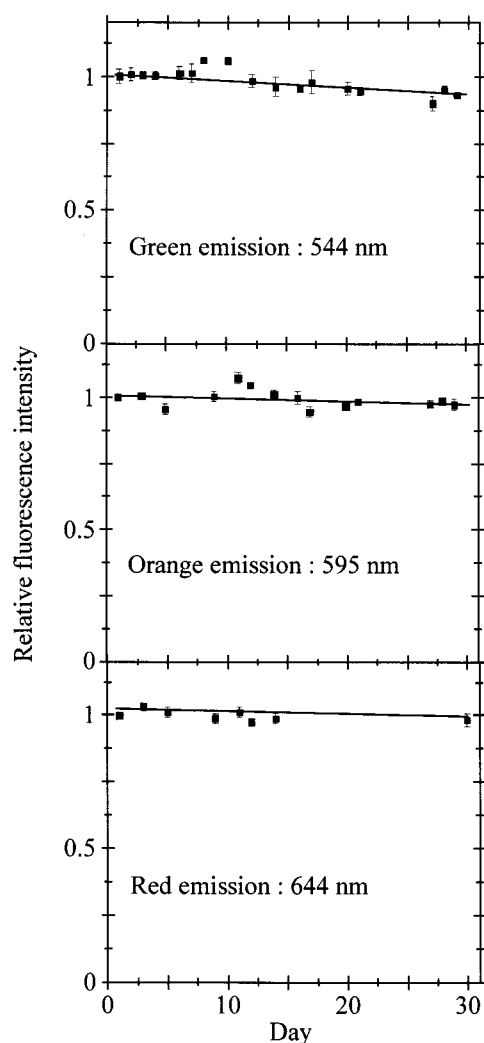


Figure 3. Time dependence of the fluorescence intensity of green, orange, and red silanized nanocrystals over time. The particles in the 10 mM PB buffer solution are excited each day and do not show an appreciable decrease of the luminescence over 1 month.

1 day. In addition, silanized nanocrystals are more stable under continuous 488 nm Ar^+ laser excitation than dye molecules. This is illustrated in Figure 4; the nanocrystal emission is almost constant over a period of 4 h, while rhodamine 6G photobleaches after 10 min under identical conditions. The nanocrystal fluorescence increased during the first minutes of illumination but then leveled off at a constant value corresponding to 120–200% of the initial value.

B. Size Characterization. Figure 5 and Table 2 report a systematic TEM–AFM study of the average size of CdSe/ZnS nanocrystals, as well as the size of silanized and MPA-coated particles from the same sample (see support information for images).

The histogram of the diameter of unsilanized yellow CdSe/ZnS nanocrystals determined by TEM is plotted at the top row of the figure. Histograms for the other color of emission are similar. The average sizes of the core/shell nanocrystals were 4.2 (0.5), 4.4 (0.4), 5.6 (0.4), and 6.4 (0.4) nm for green, yellow, red, and dark red emitting particles respectively, and the width of the distribution is nearly constant for all samples.

The silica shell on silanized nanocrystals is expected to be amorphous and should present a clear contrast with the crystalline CdSe/ZnS core/shell in HRTEM images. However, the silica shell could not be easily visualized against the ultrathin

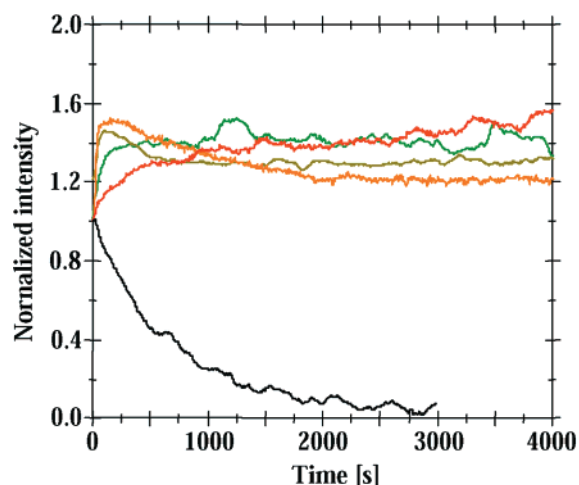


Figure 4. Time dependence of the fluorescence intensity of silanized nanocrystals and rhodamine 6G under CW Ar^+ laser radiation (0.5 mW, spot size 700 μm , volume of sample $\sim 1 \mu\text{L}$, OD = 0.065 at 488 nm). The nanocrystals exhibit a stable emission for at least ~ 4 h, while the dye bleaches after ~ 10 min. (Colors correspond to nanocrystal emission, R6G is in black.)

carbon film substrate. This difficulty suggests that the silica layer is thin and porous. Also, the small size of the core/shell particle (< 7 nm) makes the visualization of the surrounding amorphous silica shell more difficult. However, by using a lacey carbon film, we could image a particle sitting on the carbon film edge, showing an amorphous coating of ~ 3 nm (see Supporting Information).

We also performed EELS measurements (not shown) in order to characterize the silica coating. Although preliminary results suggest a selenium rich zone in the center of the nanocrystals surrounded by a silica rich shell, the size, shape, and homogeneity of the silica shell were difficult to unambiguously identify.

We used AFM to get statistical data about the silica thickness. The height of silanized nanocrystals was compared to the height of the same CdSe/ZnS nanocrystals passivated with MPA. For silica-coated nanocrystal samples, two peaks are visible in the height distribution data presented in Figure 5.^{27,28} The first peak is centered around 4 nm, regardless of the CdSe/ZnS particle size. A second peak can be discerned around 6 nm for the green emitting nanocrystals, 9 nm for yellow nanocrystals, 14 nm for red ones, and 17 nm for dark red ones. The center of this second peak is significantly bigger than the mean size of the corresponding CdSe/ZnS nanocrystals. Indeed, the increase in height is ~ 2 , 4, 8, and 10 nm for the green, yellow, red, and dark red nanocrystals, respectively. Furthermore, the width of this second peak is significantly wider than the width of the corresponding CdSe/ZnS size distribution obtained by TEM. In all cases, particles with a height larger than 20 nm are rarely observed.

In contrast, the height histograms of MPA-coated dots exhibit only one broad peak centered around 5, 5, 9, and 12 nm for green, yellow, red, and dark red emission, respectively. The average height of each MPA-coated sample is larger than the height of the corresponding CdSe/ZnS nanocrystal, but smaller than the mean height of the silanized nanoparticles forming the second histogram peak.

The AFM data do not demonstrate the degree of aggregation in the nanocrystal solution. High-performance liquid chromatography (HPLC) through a size exclusion gel is an established method to separate the components of a solution according to their size. HPLC can therefore potentially characterize the degree of aggregation in the samples.^{29,30} Particles with a diameter larger than the bead pore size do not interact with the gel and

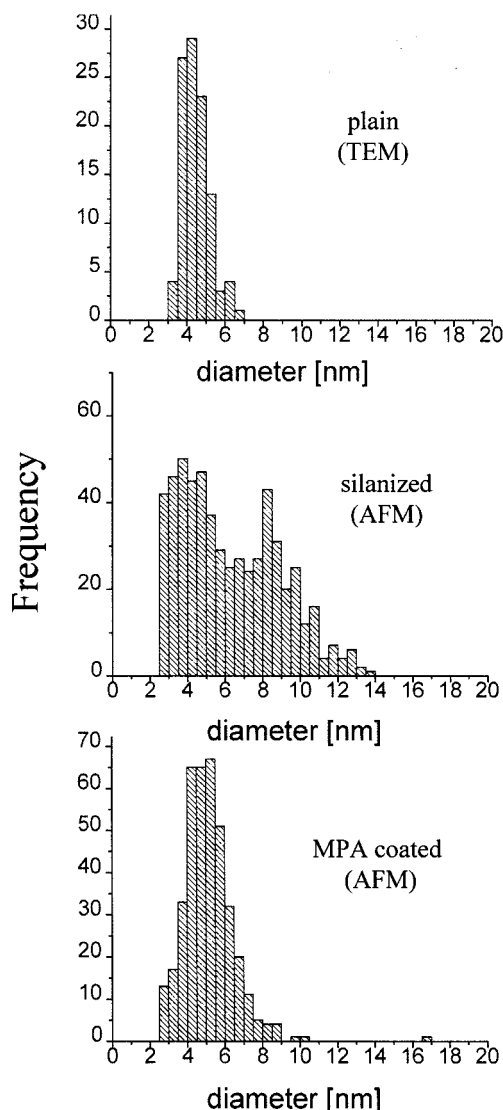


Figure 5. Size (or height distribution) of water-soluble yellow CdSe/ZnS nanocrystals. The size distribution of the core/shell CdSe/ZnS, as measured in HRTEM, is shown in the top row of the figure. The size distribution for water-soluble nanocrystals has been investigated by AFM. The silanized nanocrystals (middle row) and the MPA-coated particles are prepared from the same sample. As described in the text, the features with a height smaller than the diameter of the corresponding CdSe/ZnS nanocrystals have been omitted from the AFM histograms.

TABLE 2: Summary of the Size Characterization of the Nanocrystals^a

color of fluorescence of the nanocrystals	diameter of			
	CdSe by TEM (nm)	CdSe/ZnS by TEM (nm)	silanized CdSe/ZnS by AFM (nm)	MPA-coated CdSe/ZnS by AFM (nm)
green	2.7	4.2	6	5
yellow	3.1	4.4	9	5
red	4.1	5.6	14	9
dark red	4.8	6.4	17	12

^a The thickness of the silica shell is taken as half the difference between the diameters of CdSe/ZnS and the silica-coated nanoparticles.

elute in a void volume, while particles with a considerably smaller diameter can penetrate inside the beads and are therefore retarded.

Figure 6 shows the elution profiles of two different silanization syntheses using the same green emitting CdSe/ZnS samples. The blue line corresponds to the elution profile of a sample

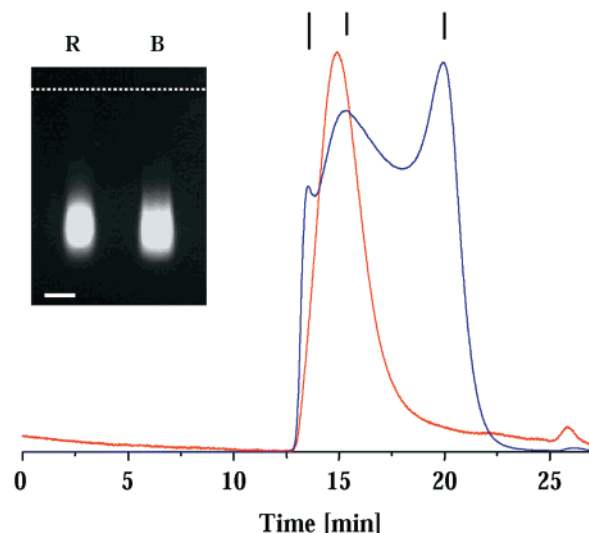


Figure 6. Chromatogram of two different silanized samples (OD \sim 0.1) run through a HPLC column and detected by UV absorption at 210 nm. The blue sample has three features indicated by the lines on the top of the figure. The feature at 13 min corresponds to the void volume containing particles larger than the pore size of the gel. The feature around 15 min corresponds to fluorescent nanocrystals. The feature around 21 min does not fluoresce and presumably contains siloxane complexes. Purification of small complexes by dialysis and repeated runs through NAP 10 columns (red curve) allow a reduction in the amount of silica present. Inset: 1% gel electrophoresis of both samples (R = red line, B = blue line) in 10 mM PB, pH = 7.2, for 40 min at 50 V shows almost identical migration patterns; the dashed line marks the loading position. Bar = 5 mm.

done in the standard way, as described in the Experimental Section. It exhibits three distinct features that have been collected separately and examined in an epifluorescence microscope. The sharp peak around 13 min corresponds to the void volume and represents \sim 8% of the area of the overall elution peak. A second feature appears at about 15 min (\sim 49% of the area) and indicates the presence of silanized nanoparticles, as evidenced by green fluorescence upon UV excitation. The last feature appears near 21 min (\sim 43% of the elution peak). It is not fluorescent, and we believe it corresponds to the excess of silica complexes. The red line corresponds to a purified sample by dialysis (MW cutoff = 100 000) and repetitive passage through a size exclusion column (NAP10) in order to get rid of smaller and bigger compounds. It exhibits only one peak. The amount of silica is notably reduced, as could be expected, and there are no nanocrystals in the void volume. Note that both samples exhibit a similar migration pattern in 1% agarose electrophoresis (inset) and cannot, therefore, be distinguished by this latter method.

C. Surface Characterization and Solubility. We have measured the number of active thiol groups ($-\text{SH}$) per nanocrystal using the Ellman's test. This number should be interpreted as an upper limit because there are still some small silica complexes in solution that can react with Ellman's reagent, and because the exact concentration of the nanoparticles is only known approximately. Our measurements reproducibly yield several hundred active thiols per nanocrystal. This number does not vary with time over a period of 1 month.

The surface charge of the nanocrystals can be probed by gel electrophoresis, since the migration driving force is electrostatic. Silanized nanocrystals have negative phosphonate groups on the surface and, therefore, migrate toward the positive electrode. A typical migration pattern in 1% agarose gel, shown in Figure 7a for the green, yellow, and red emitting nanocrystals, is usually

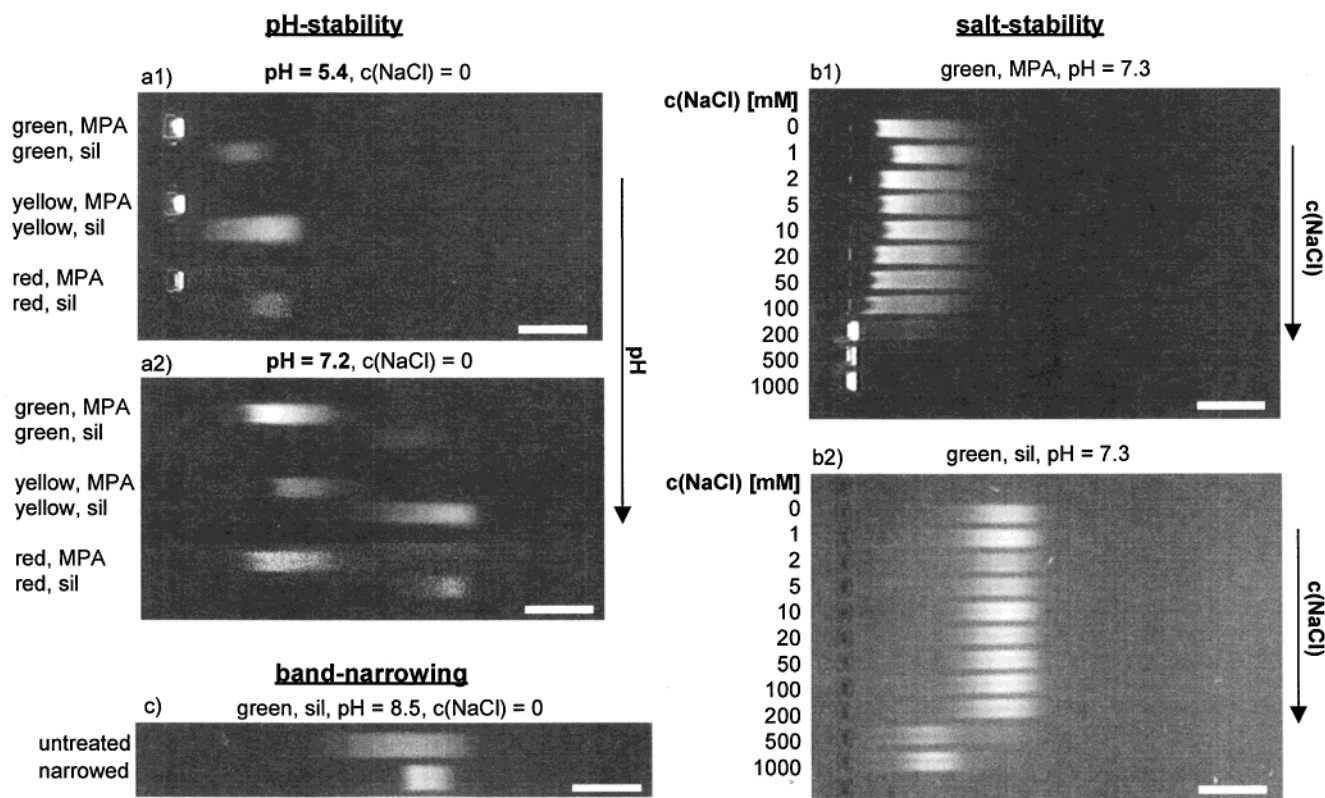


Figure 7. Gel electrophoresis of silanized and MPA-coated nanocrystals prepared from the same sample; bar = 1 cm. (a) pH stability. Particles with three different sizes (green, yellow, red emitting particles) are run in separate lanes in a 1% agarose gel for 1 h at 75 V under slightly acidic (10 mM MES buffer, pH = 5.4, no NaCl) and neutral conditions (10 mM PB buffer, pH = 7.2, no NaCl). The lanes showing the red nanocrystals have been contrast-enhanced with digital data processing. (b) Salt stability for green emitting particles. Silanized and MPA-coated nanocrystals are incubated for 5 h in 30 mM PB buffer, pH = 7.3 with different NaCl concentrations ranging from 0 to 1000 mM. They were run in 1% agarose gel for 30 min at 100 V. (c) Band-narrowing. Green fluorescent nanocrystals are run in a 1% agarose gel (50 mM TBE, pH ~ 8.6) for 1 h. With a filter paper extraction method,²⁶ particles of a small fraction of the band have been extracted from the gel. These collected particles are run again in a 1% agarose gel, in parallel with the original nanoparticles samples of same concentration.

quite broad, and strongly depends on the pH of the solution. Many features from this gel recur. First, the overall size of the silica and MPA-coated nanocrystals seems to contribute only in a minor way to the mobility of the particles. In fact, the bands of silica-coated nanocrystals for the different emission colors are approximately in the same position in Figure 7a, as the MPA-coated ones. In both neutral (pH = 7.2) and acidic (pH = 5.4) pHs, the bands of MPA-coated nanocrystals are retarded compared to the silica-coated ones. At pH = 5.4, the silanized nanocrystals exhibit a migration about half their migration at pH = 7.2, while MPA-coated nanocrystals barely show any migration. Silica and MPA-coated nanocrystals have different groups on their surface and therefore different surface charges. The surface charge can be adjusted by changing the pH of the solution, and it seems to play the major role in the mobility of particles.

As illustrated in Figure 7b, silanized and MPA-coated nanocrystals behave differently in electrolytic solutions containing high NaCl concentrations. At a given pH, silanized nanocrystal solutions are robust in high ionic strength buffers. The migration pattern of these nanocrystals is constant up to 200 mM of NaCl; at higher values, the migration is retarded. In contrast, the migration of MPA-coated nanocrystals is already reduced above 20 mM of NaCl. We point out that 200 mM of NaCl are not an upper limit for the stability of silanized nanoparticles. Other batches of particles did not show any retardation even if incubated in 1 M NaCl for 1 week.

Typical migration patterns, like the one shown in Figure 7a,b, are usually quite broad. As illustrated in Figure 7c, narrower

bands can be obtained by taking only a fraction of the nanocrystals in one band after running the gel electrophoresis, extracting this fraction from the gel and using only this selected fraction as a new sample. Yields of up to 30% have been obtained using this method.

Discussion

A. Synthesis Discussion. Ströber et al. developed a method in which SiO₂ particles can form by the hydrolysis and polycondensation of tetraethoxysilane under alkaline conditions in ethanol.³¹ Since then, various approaches, inspired by the Ströber method, have been reported to coat inorganic nanocrystals (Au,³² Ag,³³ CdS,^{19,23} CdTe,²⁰ CdSe,²⁰ and CdSe/CdS²⁰) with a silica shell. These syntheses were entirely or partially performed in water and yielded relatively thick shells of ~40–80 nm. In addition, these citrate-stabilized CdS and CdSe/CdS show a large emission from trapped states that considerably broadens their emission spectra.^{19,20,23} Monodispersed TOPO-capped CdSe/ZnS have by far superior optical properties, but they flocculate in the presence of water. The silanization method we have developed has been adapted from the previous works.^{14,19,20,31–33} It retains the narrow band emission and fairly high quantum yields of the TOPO-capped CdSe/ZnS nanoparticles and is highly reproducible. From a conceptual point of view, the procedure can be divided into two parts: the silica shell growth (including the priming, the introduction of surface charges, and the quenching step, which are represented in Figure 1), and the subsequent purification and transfer of the nanocrystals into aqueous buffers.

The silica shell growth is performed in methanol, although TOPO-capped nanoparticles are not totally soluble in this solvent.³⁴ Less polar solvents like toluene can be used to solubilize the nanocrystals and subsequently grow the silica shell. However, using toluene as a solvent has two disadvantages. First, the shell growth proceeds faster than in methanol and hence is more difficult to control. Second, we have not found any efficient and reproducible way to exchange the solvent in the final step.

In our silanization procedure (Figure 1), TOPO-capped nanocrystals are dissolved in a large excess of pure MPS. The thiol of the MPS acts as a primer on the nanoparticle surface, and the three siloxane groups act as anchor points for subsequent silica shell growth. Initially, the nanocrystals do not dissolve in MPS and produce a cloudy solution, most likely because the thiol groups of the MPS are not able to strip the TOPO molecules already adsorbed on the nanocrystal surface. The addition of a small and controlled amount of base increases the pH to 9 or 10 (checked by pH paper) and immediately generates an optically clear solution. Basification deprotonates the thiol and renders it able to compete with the TOPO ligands. Nanocrystals in MPS solution are stable for hours. However, addition of too much base drives an immediate cross-linking reaction and causes flocculation of the particles. MPS-capped nanocrystals are transferred into an almost water-free alkaline methanol solution (pH \sim 10) where they are totally soluble.³⁴ The base (TMAOH) plays a critical role since it contains a minute amount of water (<5%). Above pH \sim 8.5, H₂O molecules drive the partial hydrolysis of the trimethoxysilane groups into silanols and allow a primary polymerization due to hydrogen bonding between silanols prior to the strengthening step. The conditions chosen favor a very slow polymerization process around the nanocrystals and minimize an internanocrystal cross-linking. Mild heating ($T \sim 60$ °C) strengthens the van der Waals silanol bridges ($-\text{SiOH}\cdots\text{HOSi}-$) by converting them into covalent siloxane bonds ($-\text{Si}-\text{O}-\text{Si}-$) by releasing one water molecule.³⁵ Heating too violently ($T > 70$ °C) or too long ($\gg 1$ h) causes the flocculation of the solution, because it speeds up the polymerization rate of the silane reagents and induces internanocrystal cross-linking. The heating temperature and duration time have been empirically determined and can be varied over a broad range of values so long as the solution is not overheated.

After the first round of growth, a relatively thin silica shell formed, but the particles were not yet water-soluble. Indeed, when we removed unreacted MPS from the solution by dialyzing the solution against basified methanol, the particles flocculated after about 2 days. When the solution was dialyzed against water, the nanocrystals aggregated almost instantaneously. This behavior suggests that the silica shell is not completely cross-linked at this point and that there is still some dynamic exchange between MPS bound to the surface of the nanocrystals and free MPS in solution. Therefore, a thicker silica shell is necessary to ensure the water solubility.

This thicker shell is grown by adding fresh MPS in methanol and $\sim 10\%$ of water. Under these conditions, MPS is quickly incorporated by a silanol-silanol bridge onto the outside edge of the shell surrounding the nanocrystals. The remaining thiol and the two free silanol groups of the MPS point toward the solution, allowing the growth process to proceed. Upon addition of fresh MPS and water, the pH drops to ~ 9 and the polymerization rate slows. The consolidation of the siloxane bonds is driven again by heating for only a short period because

of the concomitant large excess of silica reagent and water in solution.

It is necessary to stop the silanization reaction to retain a thin silica shell and to prevent particle cross-linking over time. Residual alkoxy groups of the MPS on the nanocrystals are quenched by the addition of an excess of chlorotrimethylsilane. This blocks the silanol bond and thus stops the silica shell polymerization. Unquenched solutions flocculate after a few days in methanol. However, the quenching reaction introduces hydrophobic methyl groups and therefore decreases the solubility of the silanized nanocrystals in water. We have overcome this problem by adding negatively charged phosphonate groups before the quenching step. They make the primary contribution to the surface charge of the nanocrystals and, in water, favor the nanocrystal's dispersion by electrostatic repulsion. The negative phosphonate charge is indispensable to the stability of the nanocrystals in water. Our attempts to remove them resulted in precipitation of the solution after a few days.

At this point, the silica shell growth is finished and the synthesis proceeds by exchanging the solvent. The nanoparticles cannot be precipitated since the solution is too dilute. In addition, there remain a large amount of silica complexes that need to be removed. For this purpose, we first condense the solution by evaporating the solvent in a rotor evaporator or on a Schlenk line. We observe that when the concentration is too large, the solution becomes cloudy, and the particles eventually precipitate. The solution therefore is condensed by a factor of less than 4, left for at least 24 h under N₂, and then filtered through a centrifugal concentrator device to concentrate it to a volume of $\sim 2-3$ mL. The Centricon devices contain a membrane that is permeable to the solvent and small molecules (MWCO = 100 000) but not permeable to large particles such as the silanized nanocrystals. Hence, this approach allows the removal of the excess of small silica complexes. We estimate that the amount of silica is reduced by a factor of 50. The transfer to aqueous solutions is performed by using a size exclusion column filled with Sephadex G25 medium and equilibrated with either 10 mM PB buffer at pH ~ 7 or 18 MΩ Millipore H₂O. The condensed solution (~ 2 mL) is loaded directly on the top of the column. Although the top 5 mm of the Sephadex column is perturbed due to the presence of methanol, a sufficiently long column allows proper solvent exchange. Typically, we collect ~ 3 mL of a final solution containing the silanized particles in buffer. Usually, the eluted solution is slightly cloudy, most likely because the solvation of the nanocrystals in water is not immediately complete. The cloudiness can be removed by running the solution through a $0.22 \mu\text{m}$ pore size acetate filter. To purify the solution one step further, it is centrifuged at $\sim 20000\times g$ and the precipitate is discarded. The solution of silanized nanocrystals is stored in air and light and is stable for months.

After each step in the synthesis, the reagents are left for a period to allow them to reach complete equilibrium. The equilibrium times have been determined empirically. For instance, after the quenching, the solution is left for at least 2 days. Attempts to reduce this period of delay caused partial precipitation out of the solution during the condensation steps. Similarly, between the condensation step in the rotor evaporator and the final condensation stage by centrifugation, a rest time of ~ 12 h is necessary. The reason for this need is unknown. It may come from the slow solvation of the nanoparticles in the synthesis solution.

The solution of silanized nanocrystals may still contain some byproducts of the synthesis, and therefore the solutions may be

optionally dialyzed. Our purification steps should remove both excess of small complexes and large aggregates. However, we cannot exclude the presence of silica spheres having a diameter similar to the diameter of the silanized nanocrystals. The surface of the silanized nanocrystals should include the following groups: active thiols acting as anchor points for further conjugation reactions, negatively charged phosphonate groups allowing water solubility, hydrophobic methyl groups introduced during the quenching step, and unquenched silanol groups.

The silanization procedure we have described so far requires the priming of the nanocrystals with a thiolated silica precursor (MPS). Attempts to prime the nanocrystals with primary amines (APS, i.e., (aminopropyl)trimethoxysilane) have been unsuccessful. TOPO-capped nanocrystals can be dissolved in APS just as in MPS. The failure in APS priming arises after the first heating, during which the scattering of the solution increases by a factor of ~ 10 , suggesting partial agglomeration of the nanocrystals has occurred.³⁴ Although we do not know the exact reason for this behavior, it seems likely that the primary amines form a weaker bond with the Zn atoms on the ZnS surface than the bonds of the aliphatic thiols. APS can be added, however, after the priming is complete at the same time as the addition of the phosphonate reagent. APS introduces amine groups onto the nanocrystal surface and slightly increases the emission intensity.

B. Optical Characterization. Quantum yields of our silica-coated nanocrystals are about ~ 5 – 18% . Those values are in a range close to the QY of the CdSe/ZnS nanoparticles. These findings contrast with previous work,²⁰ where the fluorescence intensity of CdSe/CdS nanocrystals dropped by a factor of 20 upon silica shell growth. In that study, the emission peak dramatically broadened from a significant contribution from trapped states. The QYs of nanocrystals are smaller than the QYs of organic dyes,²⁴ but they only weakly depend on the buffer conditions. The nanocrystals' longer lifetime under continuous wave (CW) irradiation partially compensates for this overall lower emission intensity. The better stability of the nanocrystals' emission compared to that of the dyes should facilitate tracking their location over extended periods inside a cell. The main concern for applications requiring quantitative analysis may be the photobrightening of the nanocrystals under CW-laser irradiation. The fluorescence intensity increases by up to a factor of 2 in the first stage of the illumination and then levels off to a stable value. The causes of this effect are still under investigation. We stress, however, that the silica shell is not responsible for this effect since it is also observed for CdSe/ZnS nanocrystals in toluene. Photobrightening does not happen in a vacuum, suggesting that aerated solutions induce a photooxidation of the nanocrystals. This observation implies that the silica shell forms a porous matrix around the CdSe/ZnS particles. We note that aged CdSe/ZnS nanocrystals have been used throughout this study and no precautions were taken to store them. Higher QYs might be obtained using either freshly prepared CdSe/ZnS samples or double shell CdSe/CdS/ZnS nanocrystals.

C. Size Characterization. AFM data of Figure 4 show one and two features in the height histograms of the silanized and MPA-coated nanoparticles, respectively. For the silanized nanocrystal solutions, the histograms exhibit two features that should be interpreted. One hypothesis would attribute the first peak to small silica complexes and the second peak to silanized CdSe/ZnS nanocrystals. This model cannot be proved by the methods used in this study, but it is supported by many indications. The location of the first peak is at a size similar to

that of the CdSe/ZnS nanocrystals but is smaller than the size of the corresponding MPA-coated nanocrystals. Moreover, the peak appears always in the same range of sizes, regardless of the size of the starting CdSe/ZnS nanocrystals. It might be argued that this peak corresponds to CdSe/ZnS dots having only one monolayer of siloxane primer. We mentioned earlier, however, that particles after the priming step were not stable in water. This rules out the possibility of an ultrathin silica shell around the nanocrystals. Our current interpretation ascribes the first peak to small silica complexes, including silica-coated ZnS moieties.²⁸ The second peak would then be likely due to presence of silanized CdSe/ZnS nanocrystals, since the mean height becomes bigger for larger particles.

For MPA-coated nanocrystal solutions, the single peak that is present can be unequivocally ascribed to the MPA-coated nanocrystals. For green and yellow emitting particles, the MPA coating adds less than 1 nm to the diameter, which seems a plausible size for a monolayer of MPA molecules. The coating is not necessarily perfect. Especially for the green emitting nanocrystals, a tail extending to larger height can be discerned. We ascribe it to the presence of dimers and trimers. For larger MPA-coated dots (red, dark red), the mean height is clearly a few nanometers larger than the diameter of the uncoated CdSe/ZnS particles. This increase in size can no longer be explained by the presence of a single monolayer of MPA coating a single nanocrystal. It is, rather, an indication of the formation of small aggregates of particles. A further indication supporting this conclusion is the increased width of the peak in the height distribution. At this point, it is not clear whether the aggregation was already present in the solution or if it is an artifact of the deposition of the particles onto the mica.

Two problems are connected to the AFM measurements. The first is the inability to distinguish reliably between monomers, dimers, etc. The growth of the ZnS and silica shells around slightly elongated CdSe cores likely yield nonhomogeneous particles, which reduce dramatically the ability to distinguish between monomers, dimers, etc. Second, AFM is a blind probe. It does not offer the opportunity to obtain optical or chemical information about the samples. It is, therefore, impossible to directly distinguish between silica-embedded CdSe/ZnS nanoparticles and particles containing only silica. From the AFM data, we can give an upper estimate for the thickness of the silica shell. The increase in height due to the silica shell is less than 11 nm. This corresponds to a shell thickness below 5 nm and an overall particle size of 17 nm for the dark red emitting nanocrystals. As a simple interpretation, the thickness of the silica shell can be understood as half the difference between the height of silanized particles and the mean diameter of the CdSe/ZnS obtained by TEM. This would result in thicknesses of ~ 1 , ~ 2 , ~ 4 , and ~ 5 nm for green, yellow, red, and dark red emitting nanocrystals, respectively. Consequently, the AFM data indicate the presence of a silica shell 1–5 nm thick. It is obvious from the AFM measurements, that the solution contained at least two species of particles, but nearly no large aggregates (> 20 nm) were present.

The HPLC data suggests that between 90 and 100% of the silanized nanoparticles have a diameter below ~ 40 – 45 nm, which is the pore size of the beads. A size of 40 nm corresponds to approximately seven green silanized nanocrystals clustered together, or to many nanocrystals embedded inside the same silica shell. For more quantitative information, improved protocols for separation will be necessary.^{29,30} It is not possible to obtain precise numbers about the mean diameter of silanized nanoparticles from our HPLC study. To extract valuable

information about size and size distribution from the elution profiles, a model of the elution process is necessary. This model is not yet available. As a side note, it would be helpful to simultaneously measure both the fluorescence and absorption of the eluent in order to distinguish "in situ" fluorescent semiconductor species from pure silica complexes.

Conclusive characterization of the thickness/homogeneity of the silica shell in these samples turned out to be a difficult task. AFM and HPLC exclude the presence of large aggregates of nanocrystals in solution (such as several particles surrounded by a single silica shell), but it is not clear that the samples contain only monomers. There may be a fair number of dimers, trimers, twin particles (two CdSe/ZnS in a single silica shell), or triplets (three CdSe/ZnS in a single shell). However, it is important to point out that for many applications aimed to track fluorescence traces, i.e., fluorescence labeling in cells, it is not a problem if silanized nanocrystals contain one, two, three, or more cores provided the overall size of the emitting entity is small.

Concerning the shell homogeneity, it is unlikely that the particles have an imperfect shell (partial covering). Partially coated particles probably would be less stable in water. They would agglomerate during the many purification steps and would not be present in the final solution.

D. Surface Characterization. The migration patterns, shown in Figure 7a,b, are quite broad, indicating most likely a wide charge distribution under these electrophoresis conditions. We exclude the mass distribution as a primary source of the broadening since MPA-coated nanocrystals, which have a more uniform size distribution, exhibit a similar broadening. We explain this behavior by noting that the isoelectric point of nanocrystals in solution depends on the exact surface composition. In this respect, the carboxyl groups of the MPA-coated particles have almost no charge around $\text{pH} = 5.4$, as evidenced by the gel in Figure 7a, while silanized nanocrystals remain negatively charged between $\text{pH} = 5.4$ and $\text{pH} = 8.6$. The presence of a large amount of negative charge ensures the long-range repulsive interactions between nanocrystals that overwhelm their short-range van der Waals attractions. The stability of the nanocrystal solutions over a wide range of buffer conditions is an important factor for bioconjugation and the use of inorganic nanocrystals as fluorescent probes in biology. Unlike silanized nanocrystals, MPA-coated particles do not withstand these conditions fully. Silica-coated nanocrystals offer another advantage over the MPA-coated ones. In silanized nanocrystals, the phosphonate groups are responsible for the nanocrystals' stability, while the thiol groups serve as anchor points for bioconjugation. In contrast, in MPA-coated dots, the carboxyl groups play a double role. Separation of the stabilizing and reactive functional groups is clearly desirable; if neutral biomolecules were attached to MPA-coated nanocrystals, fewer free carboxyl groups would remain on the surface, and the stability of the solution would suffer.

Control of the surface properties of the silanized nanocrystals is difficult. Our synthesis consistently yields several hundred active thiols per particle and an unknown number of negatively charged phosphonate groups. The large number of thiols is desirable for allowing further derivation with biomolecules using the previously established bioconjugation techniques.²⁵ The surface charge, however, is more difficult to control. The wide charge distribution considerably broadens the gel electrophoresis bands and precludes the isolation of several species. It is of interest for nanoconstruction to isolate nanocrystals containing precise numbers of single strands of DNA.²⁶ Such a counting

has been performed for gold colloids,³⁶ and it would constitute an important technology for semiconductor nanocrystals, too. Silanized nanocrystal bands can be sharpened by electrophoresis, as shown in Figure 7c. Although such a yield is relatively low, electrophoresis is a viable compromise while we await an improved silanization technique.

Conclusion

We have reported a procedure to embed CdSe/ZnS of various sizes into a silica bead and simultaneously introduce biological functional groups. The silanized nanocrystals retain the optical properties of the original CdSe/ZnS cores and can have emission colors from blue to dark red with a fwhm of ~ 32 nm. The silanized solutions have quantum yields of a few tens of percent and are stable for months. The best nanocrystals survive intense laser illumination for hours and, therefore, represent an important improvement compared to organic fluorophores.

Silanized nanocrystals have similar optical properties to MPA-coated ones. The latter are by far easier to prepare, but unlike silanized particles, they exhibit poor stability in buffers under physiological conditions. Conjugation of the nanocrystals with biologically relevant molecules requires these conditions. Silanized nanoparticles present an important advance in that direction. Our most recent work, focusing on the covalent coupling of single strands of DNA to the semiconductor nanocrystals, indicates that silanized particles are definitively easier to handle than the MPA-coated ones. Silanized nanocrystals that are covalently coupled to oligonucleotides open a route toward the synthesis of programmable assemblies of nanocrystals, and they may ultimately replace the organic dyes in some fluorescence detection experiments.

Acknowledgment. We thank both Dr. Marcel Bruchez and Brian Gin for valuable suggestions and discussions, Dr. Jiangtao Hu for the assistance with the epifluorescence microscope, Chris Nelson for the help with EELS measurements, and Carolin Toksford for helpful comments about the AFM measurements. We also thank the NCEM-Lawrence Berkeley National Laboratory and LME-Laboratório Nacional de Luz Síncrotron (Campinas, Brazil) for the use of TEMs. D.G. thanks the Swiss National Science Foundation (FNS) for financial support. S.C.W. acknowledges the Lawrence Livermore National Laboratory and the National Physical Science Consortium. W.J.P. is supported by the German Research Foundation (DFG), and D.Z. is grateful to FAPESP, proc. 99/08603-7. This work was supported by the NIH National Center for Research Resources, Grant 1 R01 RR-14891-01 through the U.S. Department of Energy under Contract No. DE-AC03-76SF00098, by the DOD Advanced Research Projects Agency (DARPA) under Grant No. N00014-99-1-0728, and (in part) by the Director, Office of Energy Research, Office of Science, Division of Materials Sciences, of the U.S. Department of Energy under Contract No. DE-AC03-76SF00098.

Supporting Information Available: HRTEM and AFM figures of silanized nanocrystals. This material is available free of charge via the Internet at <http://pubs.acs.org>.

References and Notes

- (1) Murray, C. B.; Norris, D. J.; Bawendi, M. G. *J. Am. Chem. Soc.* **1993**, *115*, 8706.
- (2) See also a recent review: Murray, C. B.; Kagan, C. R.; Bawendi, M. G. *Annu. Rev. Mater. Sci.* **2000**, *30*, 545.
- (3) Peng, X.; Manna, L.; Yang, W.; Wickham, J.; Scher, E.; Kadavanch, A.; Alivisatos, A. P. *Nature* **2000**, *404*, 59.
- (4) Manna, L.; Scher, E. C.; Alivisatos, A. P. *J. Am. Chem. Soc.* **2000**, *122*, 12700.

- (5) Welser, J. J.; Tiwari, S.; Rishton, S.; Lee, K. Y.; Lee, Y. *IEEE Electron Device Lett.* **1997**, *18*, 278.
- (6) Murray, C. B.; Kagan, C. R.; Bawendi, M. G. *Science* **1995**, *270*, 1335.
- (7) Huyhn, W.; Peng, X.; Alivisatos, A. P. *Adv. Mater.* **1999**, *11*, 923.
- (8) Vlasov, Y. A.; Yao, N.; Norris, D. J. *Adv. Mater.* **1999**, *11*, 165.
- (9) Efros, A. L.; Rosen, M. *Annu. Rev. Mater. Sci.* **2000**, *30*, 475.
- (10) Nirmal, M.; Brus, L. *Acc. Chem. Res.*, **1999**, *32*, 407.
- (11) Dabbousi, B. O.; Rodríguez-Viejo, J.; Mikulec, F. V.; Heine, J. R.; Mattoussi, H.; Ober, R.; Jensen, K. F.; Bawendi, M. G. *J. Phys. Chem. B* **1997**, *101*, 9463.
- (12) Hines, M. A.; Guyot-Sionnest, Ph. *J. Phys. Chem.* **1996**, *100*, 468.
- (13) Peng, X.; Schlamp, M. C.; Kadavanich, A. V.; Alivisatos, A. P. *J. Am. Chem. Soc.* **1997**, *119*, 7019.
- (14) Bruchez, M. J.; Moronne, M.; Gin, P.; Weiss, S.; Alivisatos, A. P. *Science* **1998**, *281*, 2013.
- (15) Chan, W. C. W.; Nie, S. *Science* **1998**, *281*, 2016.
- (16) Tsurui, H.; Nishimura, H.; Hattori, S.; Hirose, S.; Okamura, K.; Shirai, T. *J. Histochem. Cytochem.* **2000**, *48*, 653.
- (17) Nirmal, N.; Norris, D. J.; Kuno, M.; Bawendi, M. G.; Efros, A. L.; Rosen, M. *Phys. Rev. Lett.* **1995**, *75*, 3728.
- (18) Dahan, M.; Laurence, T.; Pinaud, F.; Chemla, D. S.; Alivisatos, A. P.; Sauer, M.; Weiss, S. *Opt. Lett.*, submitted for publication.
- (19) Correa-Duarte, M. A.; Giersig, M.; Liz-Marzan, L. M. *Chem. Phys. Lett.* **1998**, *286*, 497.
- (20) Rogach, A. L.; Dattatri, N.; Ostrander, J. W.; Giersig, M.; Kotov, N. A. *Chem. Mater.* **2000**, *9*, 2676.
- (21) Mitchell, G. P.; Mirkin, C. A.; Letsinger, R. L. *J. Am. Chem. Soc.* **1999**, *121*, 8122.
- (22) Chen, C. C.; Yet, C. P.; Wang, H. N.; Chao, C. Y. *Langmuir* **1999**, *15*, 6845.
- (23) Mulvaney, P.; Liz-Marzan, L. M.; Giesig, M.; Ung, T. *J. Mater. Chem.* **2000**, *10*, 1259.
- (24) Kubin, R. F.; Fletcher, A. N. *J. Lumin.* **1982**, *27*, 455.
- (25) Hermanson, G. T. *Bioconjugation Techniques*; Academic Press: 1996.
- (26) Loweth, C. J.; Caldwell, W. B.; Peng, X.; Alivisatos, A. P.; Schultz, P. G. *Angew. Chem., Int. Ed. Engl.* **1999**, *38*, 1808.
- (27) For every water-soluble sample (silanized and MPA-coated nanocrystals), the AFM histograms indicate a prominent peak between 0.5 and 2 nm. We ascribe this feature mainly to small silica complexes and small ZnS particles produced during the ZnS shell growth that have not been removed from the solution.²⁸ Since this peak does not give information about the thickness of the silica shell, it is omitted in the histogram for clarity. Therefore, in Figure 5, we arbitrarily omit the particles with a height lower than the diameter of the corresponding CdSe/ZnS nanocrystals.
- (28) The presence of residual small ZnS particles in solution is investigated in different ways. First, the absorption spectrum of CdSe/ZnS core/shell shows a sharp exciton feature in the UV range. Precursors for the ZnS shell growth are injected in a hot pure TOPO to simulate a shell growth, but no CdSe cores are present in the solution. The absorption spectra of this test solution exhibit in the UV the same sharp exciton feature observed for our CdSe/ZnS particles. This absorption peak in the UV is also found in stock solutions for the ZnS shell growth kept at room temperature for a few days. The fraction of small particles found in solutions of silica and MPA-coated nanocrystals is therefore ascribed to small ZnS particles produced during the ZnS shell growth.
- (29) Fisher, Ch. H.; Weller, H.; Katsikas, L.; Henglein, A. *Langmuir* **1989**, *5*, 429.
- (30) Wilcoxon, J. P.; Martin, J. E.; Provencio, P. *Langmuir* **2000**, *16*, 9912.
- (31) Ströber, W.; Fink, A.; Bohn, E. *J. Colloid Interface Sci.* **1968**, *26*, 62.
- (32) Liz-Marzan, L. M.; Giersig, M.; Mulvaney, P. *Langmuir* **1996**, *12*, 4329.
- (33) Ung, T.; Liz-Marzan, L. M.; Mulvaney, P. *Langmuir* **1998**, *14*, 3740.
- (34) Qualitative information about the scattering of the solution, and hence about the average size of the components in the solution, can be obtained with the fluorometer setup. The second harmonic of the excitation wavelength is scattered isotropically by the solution. The light scattered at 90° is measured with the fluorometer detector. CdSe/ZnS nanocrystals in methanol have a scattered light intensity almost 100 times larger than in toluene. This effect cannot be ascribed to the difference in the refractive index of methanol and toluene. CdSe/ZnS nanocrystals in methanol primed with MPS do not exhibit any scattering.
- (35) Plueddemann, E. P. *Silane Coupling Agents*, 2nd ed.; Plenum Press: New York, 1991.
- (36) Zanchet, D.; Micheel, C.; Parak, W. J.; Gerion, D.; Alivisatos, A. P. *Nano Lett.* **2001**, *1*, 32.